Journal of Electroceramics 3:2, 195–212, 1999

High Transition Temperature Superconducting Quantum Interference Devices: Basic Concepts, Fabrication and Applications

DIETER KOELLE

II. Physikalisches Institut, Lehrstuhl für Angewandte Physik, Universitäat zu Köln, Zülpicherstr. 77, D-50937 Köln, Germany
E-mail: koelle@ph2.uni-koeln.de

Abstract. The performance of superconducting quantum interference devices (SQUIDs) and SQUID based magnetometers made from thin films of high transition temperature superconductors (HTS) has greatly improved since the discovery of HTS more than a decade ago. This fact is related to a steady improvement in the fabrication technology for HTS thin films and Josephson junctions. The state-of-the-art in HTS SQUID fabrication, device concepts and applications is briefly reviewed.

Keywords: superconducting quantum interference devices, high transition temperature superconductors, thin films

1. Introduction

Superconducting quantum interference devices (SQUIDs) are the most sensitive detectors for magnetic flux. SQUID based magnetometers, made from thin films of low temperature superconductors (LTS), operate at $T = 4.2$ K, the boiling temperature of liquid helium (LHe). These devices achieve an unrivaled magnetic field resolution, on the order of some fT/Hz$^{1/2}$ down to frequencies below 1 Hz. This sensitivity is adequate for most demanding applications in magnetometry, like magnetoencephalography (MEG), which is based on measuring tiny signals generated from the human brain.

The discovery of high transition temperature superconductors (HTS) by Bednorz and Müller [1] in 1986 and the observation of transition temperatures (T_c) above $T = 77$ K, the boiling point of liquid nitrogen (LN_2), opened the perspective to operate LN_2-cooled SQUIDs based on these ceramic oxides. Since LN_2 boils away much more slowly than LHe, cryogenic requirements are significantly relaxed. This lead to the perception that HTS SQUIDs, if fabricated on the basis of a HTS thin film technology, may eventually be used for more widespread applications, and this initiated considerable activities to develop sensitive HTS thin film SQUIDs.

A SQUID is a superconducting ring, intersected by one or two Josephson junctions [2,3]. Its output is a periodic function of the applied magnetic flux Φ threading the SQUID loop, with a period of one flux quantum $\Phi_0 \simeq 2.07 \times 10^{-15}$Vs. Measuring magnetic field, rather than flux, requires an appropriate input circuit, e.g., a flux transformer to enhance the SQUID's sensitivity to magnetic fields. Such a flux transformer is a closed superconducting loop and contains basic elements of a thin film multilayer technology: crossovers and vias, that is, intersecting superconducting lines separated by an insulating layer and superconducting interconnects between two superconducting layers. Hence, SQUIDs with proper input circuits contain all basic ingredients of more complex superconducting electronics circuits: thin superconducting films, Josephson junctions and patterned multilayer structures with superconducting and insulating thin films. Therefore many research groups focused on the SQUID as a basic device to develop a HTS thin film technology, which eventually might be applicable to more complex HTS circuits as well.

The intrinsic sensitivity of a SQUID is limited by the spectral density of its flux noise, which is white at high frequencies and scales as $1/f$ below a threshold frequency. The white noise depends on operating

temperature T and basic SQUID parameters, as the critical current I_0 and the resistance R of the Josephson junctions and the inductance L of the SQUID loop. The $1/f$ noise arises mainly from fluctuations in the critical current I_0 of the Josephson junctions and from flux noise induced by vortex motion in the film. While the noise due to I_0 fluctuations can be largely reduced by appropriate read-out schemes, the low frequency flux noise from vortex motion can not be reduced electronically, and it has been shown that it is strongly correlated with film quality.

Key technological requirements for sensitive SQUIDs and magnetometers are the reliable fabrication of *superconducting films with low 1/f noise* and *Josephson junctions with reproducible parameters*. For more advanced designs *patterned multilayer structures with low 1/f noise* are required, which have to include well defined Josephson junctions in integrated devices.

The nature of the cuprate superconductors, namely their strong sensitivity to chemical and structural changes on atomic length scales, leads to a strong sensitivity of their transport and noise characteristics on microstructure and defect structure. E.g., high angle grain boundaries strongly depress the critical current and enhance vortex motion. Very early in the stage of the field in became evident that epitaxial growth of single crystal HTS films on lattice matched substrates is essential to avoid such defects, and to accomplish the requirements mentioned above.

If compared to LTS SQUIDs, the fabrication of sensitive HTS SQUIDs faces two major problems: Firstly, $1/f$ noise due to vortex motion is high because thermal energy at 77 K is much higher and pinning energies are lower. Secondly, due to the above-mentioned strong sensitivity to defects, the reproducible fabrication of Josephson junctions, i.e., two superconducting electrodes separated by a weak link (e.g., an insulating tunnel barrier), with well defined interfaces on atomic scale, is quite challenging. Both are major issues for a successful HTS thin film technology. The performance of thin film HTS SQUIDs and SQUID based magnetometers has greatly improved after the first devices have been made. This fact is related to a steady improvement in the fabrication technology for HTS thin films and Josephson junctions.

This brief review is aimed to give an overview on the state-of-the-art in HTS SQUID fabrication, device concepts and applications. It starts in section 2 with an overview of basic device concepts. In sections 3 and 4 HTS thin film technology and fabrication of Josephson junctions will be discussed, before the performance of practical devices is presented in section 5. Finally, some examples of HTS SQUID applications will be given in section 6. Due to limitations in space, this review can only give some basic ideas on device concepts and mention key issues for their realization. For more details on various aspects of SQUIDs, the interested reader is referred to the book edited by H. Weinstock [4]. A more extensive, recent review on HTS SQUIDs is given in [5].

2. Device Concepts

The SQUID combines two macroscopic quantum phenomena, namely flux quantization in a superconducting ring [6,7] and the Josephson effect in one or two weak links intersecting the SQUID loop. An applied flux Φ threading the loop gives an output, which is typically read out as a voltage, which is a periodic function of Φ with a period of Φ_0. The spectral density of flux noise is $S_\Phi(f) \equiv S_V(f)/V_\Phi^2$, where $S_V(f)$ is the spectral density of voltage noise and $V_\Phi \equiv \partial V/\partial\Phi$ is the transfer coefficient. The noise energy per unit bandwidth is $\varepsilon \equiv S_\Phi/2L$. Basic constraints on the SQUID parameters can be derived in the white (thermal) noise limit:

- To maintain flux quantization the magnetic, the Josephson coupling energy per flux quantum $\Phi_0^2/2L$ should be above the thermal energy k_BT, which sets an upper limit on the SQUID inductance $L \lesssim L_{th} \equiv \Phi_0^2/4\pi k_BT$ ($L_{\rm th} \approx 320\,{\rm pH}$ at $T = 77\,{\rm K}$). Hence, the higher operation temperature of HTS SQUIDs requires smaller inductance. This makes optimization of magnetometers very difficult since one has to compromise between optimum noise performance (small L) and good input coupling (large L).
- To maintain the Josephson coupling, the Josephson coupling energy $E_J \equiv 2\pi k_BT/I_0\Phi_0$ should be above the thermal energy, which sets a lower limit on the maximum Josephson current $I_0 \gtrsim I_{th} \equiv 2\pi k_BT/\Phi_0$ ($I_{th} \approx 3.3\mu{\rm A}$ at $T = 77\,{\rm K}$), which increases with temperature. LTS SQUIDs are operated with typical values for the noise parameter $I_{th}/I_0 \equiv \Gamma \approx 0.05$. For HTS SQUIDs Γ often is significantly higher [5].

Obviously, thermal fluctuations are a much bigger issue for HTS SQUIDs than for LTS SQUIDs and

have to be taken into account for modeling and optimizing the performance of HTS SQUIDs.

2.1. Dc SQUID

The dc SQUID [8] contains two Josephson junctions intersecting its loop. The junctions should have a non-hysteretic current-voltage-characteristic (IVC), described by the resistively shunted junction (RSJ) model [9,10]. A monotonic change in Φ causes a modulation of the SQUID's critical current I_c. If the SQUID is biased at a constant current I_B close to I_c, the periodic V-Φ-pattern is obtained, as shown in Fig. 1. To measure a small change in flux $\delta\Phi \ll \Phi_0$, one generally sets I_B to get maximum amplitude of the voltage modulation and then fixes the external flux at $(2n+1)\Phi_0/4$, to obtain the maximum transfer coefficient $\partial V/\partial\Phi$, which is denoted as V_Φ.

Numerical simulations in the thermal noise limit for LTS dc SQUIDs with representative parameters ($\Gamma \approx 0.05$) predict optimum performance for $\beta_L \equiv 2LI_0/\Phi_0 \approx 1$ [11]. In this case $V_\Phi \approx R/L$, $S_V \approx 16k_BTR$, and $\varepsilon \approx 9k_BTL/R \approx 9k_BT\Phi_0/2I_0R$. Thus the noise power increases linearly with temperature and $(I_0R)^{-1}$, which requires Josephson junctions with large I_0R-products. Similar simulations for HTS dc SQUIDs [12–14] predict also optimum performance for β_L close to one, but show a severe degradation in V_Φ for L above 50–60 pH at $T = 77$ K.

The analytic approach by Chesca [15,16] in the limit $\beta_L \leq 1/\pi$ (equivalent to $L/L_{th} \leq \Gamma/\pi$) is expected to give an adequate description for dc SQUIDs under the presence of very large thermal fluctuations, while the numerical simulations treat the thermal noise as a small perturbation. Both theories predict a strong deterioration of transfer coefficient and noise for the dc SQUID if the values for either Γ or L/L_{th} approach one.

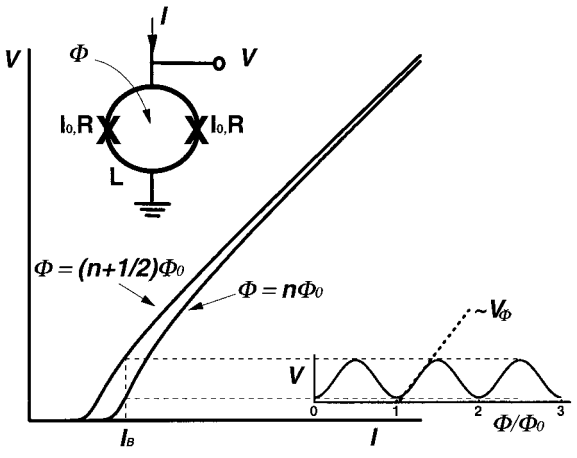

Fig. 1. I-V characteristic of dc SQUID for two values of Φ (n: integer). Insets show dc SQUID schematically (upper left) and $V(\Phi)$-pattern for constant I_B (lower right).

2.2. Rf SQUID

The rf SQUID [17–19] contains only one Josephson junction in the SQUID loop [Fig. 2(a)]. An LC-resonant tank circuit is inductively coupled to the SQUID and driven by an rf current of frequency ω_{rf} at or close to the resonance frequency, typically some ten MHz up to 1 GHz. The applied flux Φ modifies the total flux Φ_T in the SQUID loop according to $\Phi_T = \Phi - LI_0 \sin(2\pi\Phi_T/\Phi_0)$. Rf SQUIDs operate in two different modes, depending on the value for $\tilde{\beta}_L \equiv 2\pi\beta_L$.

If $\tilde{\beta}_L > 1$, negative values of the slope $\partial\Phi_T/\partial\Phi$ give a hysteretic $\Phi_T(\Phi)$ characteristic. In the *hysteretic mode* the rf flux applied by the tank circuit induces jumps between flux states in the SQUID loop [arrows in Fig. 2(b)] which leads to dissipation of energy that is extracted from the tank circuit. This in turn leads to a modulation of the quality factor Q of the tank circuit and hence to a modulation of the rf voltage across the tank circuit, which is periodic in Φ, with a period of Φ_0. Sufficient coupling between SQUID and tank circuit requires $\kappa Q^2 \gtrsim 1$ (κ: coupling constant). For fixed κQ^2, the transfer coefficient scales with ω_{rf}, $Q^{1/2}$ and $L^{-1/2}$ [20]. Hence increasing ω_{rf} and Q improves performance.

In contrast to the dc SQUID, the noise contribution from the room-temperature preamplifier can be substantial. Therefore the energy resolution ε depends on thermal noise *and* on preamplifier noise [20]. Most important, ε scales as $1/\omega_{rf}$, and the preamplifier noise typically dominates for representative values of LTS rf SQUIDs. However, raising the temperature from 4.2 K to 77 K, the preamplifier noise should not increase very much, which makes HTS rf SQUIDs quite attractive, particularly if ω_{rf} is raised up to the GHz range, as has been done over the past few years.

In the *nonhysteretic mode* ($\tilde{\beta}_L < 1$) the junction phase transitions are dispersive, and there is no noise associated with flux jumps, as for the hysteretic case. The transfer coefficient is modified by a factor

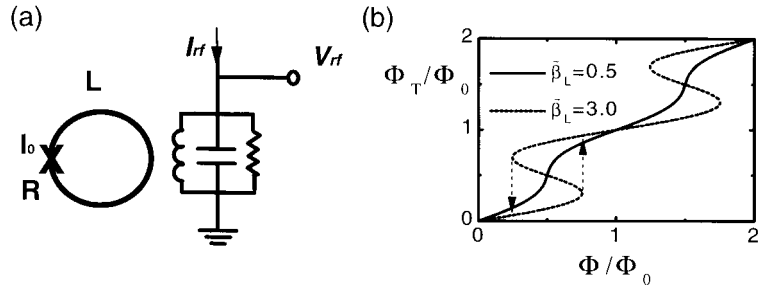

Fig. 2. (a) The rf SQUID, (b) Φ_T vs. Φ characteristic.

$\tilde{\beta}_L\sqrt{\kappa^2 Q}$ as compared to the hysteretic mode [5], resulting in substantially larger V_Φ if $\kappa^2 Q \gg 1$. Recently the performance of non-hysteretic rf SQUIDs under the presence of large thermal fluctuations has been investigated theoretically by Chesca [21]. His analytic theory predicts $\varepsilon \propto \Gamma^2$ for values of Γ on the order of one and for values of $L/L_{th} \gtrsim 0.1$. Hence for large Γ the rf SQUIDs appear to be superior to dc SQUIDs, where $\varepsilon \propto \Gamma^4$ is expected for large Γ (in the limit $\beta_L < 1/\pi$). Secondly, Chesca finds optimum values $\tilde{\beta}_L = 1$ if $\Gamma \leq 1$ and $\tilde{\beta}_L = 1/\Gamma$ if $\Gamma \geq 1$. For the latter case the optimum inductance is approximately equal to $L_F \equiv L_{th}/\pi$, which is approximately 100 pH at $T = 77$ K. This explains why optimum HTS rf SQUIDs can be operated with larger inductances than HTS dc SQUIDs, which may be a significant advantage, particularly for magnetometers (section 2.3.1).

2.3. Input Circuits

The high sensitivity of SQUIDs can be used to measure any physical quantity which can be converted into magnetic flux via an appropriate input circuit. Most SQUIDs, however, are used as magnetometers or gradiometers. That is they are coupled to input circuits which convert magnetic field or field gradient into magnetic flux.

2.3.1. Magnetometers. The figure of merit for magnetometer input circuits is the effective area $A_{eff} \equiv (\partial B/\partial\Phi)^{-1}$. The magnetic field resolution is given as $S_B \equiv S_\Phi/A_{eff}^2$. Hence an obvious task is to provide an input circuit that gives maximum increase of A_{eff} while S_Φ is kept as small as possible. For LTS SQUIDs the standard approach is based on input circuits fabricated with a well established low noise thin film multilayer technology. The situation for HTS SQUIDs however proved to be much more difficult, since input circuits based on multilayer structures tend to induce significant low frequency noise. Therefore a variety of input structures based on both, single layer and multilayer HTS films have been investigated [Fig. 3].

The large washer SQUID [Fig. 3(a)] is based on the flux focussing effect of the SQUID washer [22]. Its

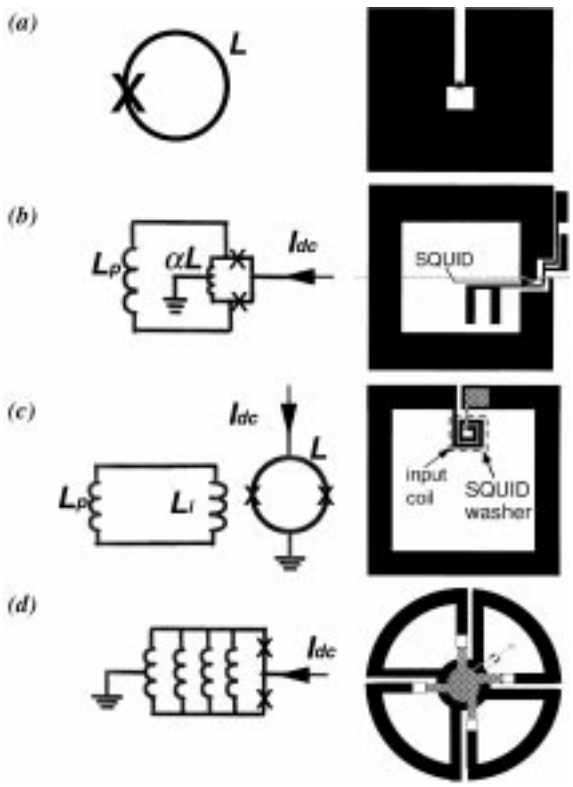

Fig. 3. Types of magnetometers: (a) large washer SQUID; (b) directly-coupled magnetometer; (c) flux transformer coupled SQUID; (d) multiloop SQUID.

effective area scales about linearly with inner hole size and outer dimension of the washer. While large washer SQUIDs have been used most successfully for HTS rf SQUIDs, another single layer approach, the directly-coupled magnetometer [Fig. 3(b)], is most often used for dc SQUIDs. This design consists of a large pickup loop of inductance L_p, which is connected to a large fraction α of the SQUID inductance L. A magnetic field applied to the pickup loop induces a screening current that is directly injected into the SQUID body. However, the flux coupling is quite inefficient since L_p is typically much larger than L. Matching between pickup loop inductance and SQUID inductance is optimized by using a flux transformer [23,24] with a large pick-up loop connected to a multiturn spiral input coil of inductance L_i that is inductively coupled to a washer SQUID [Fig. 3(c)]. The fabrication of a superconducting connection between the innermost turn of the spiral input coil and the pickup loop requires a thin film multilayer technique. For HTS magnetometers most often the flux transformer is fabricated on a separate chip and coupled to the SQUID in flip-chip configuration. This allows to separate the critical issues of optimizing SQUID performance, which is mostly an issue of optimum junction parameters, from optimizing the multilayer process with respect to low $1/f$ noise. A second multilayer magnetometer approach uses the multiloop magnetometer [25–27]. The basic idea is to connect N loops in parallel, to reduce the inductance of the SQUID to an acceptable level while the effective area is kept large [Fig. 3(d)].

Single layer HTS magnetometers have been quite successful at a time when multilayer HTS magnetometers showed much higher noise levels at 1 Hz, due to $1/f$ noise from vortex motion. Progress in the field of multilayer magnetometers was strongly connected to progress in film technology, which will be discussed in section 3.

2.3.2. Gradiometers. Many applications require the measurement of field gradients or the detection of weak signals from localized sources against a large background magnetic noise. If magnetic shielding is not appropriate, gradiometers in various configurations are used to measure first order gradients $(\partial B_i/\partial x_j; i,j = 1,2,3)$ and gradients of higher order. Two basically different approaches exist. One may either take the output of single magnetometers and use electronic or software subtraction. However this approach demands a very large dynamic range and slew rate [28], if strong disturbances are present. Alternatively one can subtract the magnetic fields at different locations directly in the pickup structure and feed the difference signal to the SQUID. The latter is the standard approach in LTS technology, based on Niobium wire wound pickup loops, mounted on a common axis to measure $\partial B_z/\partial z$ or $\partial^2 B_z/\partial z^2$. Such axial gradiometer configurations are not feasible with HTS technology, due to the lack of a suitable superconducting wire. Therefore, HTS axial pickup structures require electronic or software formation of gradiometers. As an alternative, planar thin film devices measure off-diagonal gradients e.g., $\partial B_z/\partial x$. A drawback however is the relatively short baseline, which is limited by the size of the substrate.

3. Thin Film Technology

The fabrication and micropatterning of thin films is a basic prerequisite for the realization of sensitive SQUIDs and proper input circuits. As mentioned in the earlier sections, such a HTS thin film technology faces severe problems, due to the specific nature of these materials. Key requirements for the films are high crystalline quality to provide good electrical transport properties and efficient flux pinning. For the preparation of multilayer structures it is essential to achieve heteroepitaxial growth of superconducting and insulating layers. Therefore these materials must have comparable lattice constants and thermal-expansion coefficients. They have to be chemically compatible at the relatively high deposition temperatures, and they must be deposited with sufficiently smooth surfaces to allow subsequent layers to grow with high structural and electrical integrity. Moreover, ex-situ photolithographic patterning of the various layers, that is between different deposition steps, has to be performed without introducing a significant deterioration in thin film properties, particularly at the film surface and patterned edges.

Throughout the last decade, $YBa_2Cu_3O_{7-\delta}$ (YBCO) with $T_c \approx 90$K [29] has become the material of choice for fabrication of practical HTS SQUIDs. This is mainly due to the fact that its physical properties and growth mechanisms are relatively well understood and high-quality thin films can be grown

epitaxially by a variety of deposition techniques on a number of substrate materials. Most important, only c-axis oriented YBCO films have been shown to provide sufficiently low levels of 1/*f* noise. Among a wide variety of suitable substrate materials [30], (100) $SrTiO_3$ and $LaAlO_3$ are the most widely used. However the large dielectric constant of $SrTiO_3$ (STO) can lead to parasitic resonances and adds a significant stray capacitance to the junction capacitance C, which can drive the junctions into the hysteretic limit, particularly if I_0R is high. Furthermore its high dielectric losses prevents STO from being used for high Q superconducting resonators for rf SQUIDs. $LaAlO_3$ undergoes a phase transition upon cooling to room temperature, which makes this material not suitable for multilayer patterning, since the twinning associated with the phase transition causes displacements in micropatterned structures. Hence, the ideal substrate material for HTS SQUID fabrication has not been found yet.

3.1. Thin Film Deposition and Properties

Various techniques have been used to deposit YBCO films [31,32], however the most commonly used for SQUID fabrication are pulsed laser deposition and magnetron sputtering. The c-axis films usually 100–200 nm thick are typically grown in an oxygen depleted, tetragonal phase at substrate temperatures $T_s \approx 700 - 800°C$ in 0.1-1mbar O_2, and formation of the superconducting, fully oxygenated, orthorhombic phase occurs during cooling to room temperature in 0.5-1 atm O_2. Smooth YBCO films with rms roughness around 1 nm can be obtained, and critical current densities at 77 K of up to $6 \times 10^6\,Acm^{-2}$ are two orders of magnitude higher than in high-quality YBCO single crystals. This indicates that a high density of defects, which provide strong pinning sites, must be present. However, it is not known yet what kind of defects act as effective pinning sites and how formation of these defects can be controlled.

Metallization of Au or Ag contact pads is usually done by thermal evaporation, electron-beam evaporation, or sputtering with the substrate at room temperature. A low metal/YBCO contact resistance ($< 10^{-6}\Omega cm^2$) can be achieved if the metal layer is deposited either in-situ or after only a brief exposure to air [33].

3.2. Patterning

Patterning the thin films to form linewidths on a micrometer or even submicron scale is essential for the realization of SQUIDs and input circuits. Key issues are on the one hand the possible degradation of the film surface which is detrimental to epitaxial multilayer growth, and on the other hand the quality and shape of the patterned edges. The latter significantly influences the subsequent growth of films over these edges and controls vortex entry into the film, which e.g., has impact on hysteresis in SQUIDs and on 1/*f* noise. Contact of YBCO with water or water-soluble chemicals degrades the superconducting properties and has to be avoided. The use of dry etching methods in vacuum can lead to a significant heating of the sample and thus to oxygen loss at the edges. Given these limitations, however, a number of techniques have been used to pattern YBCO films [32,34].

Conventional photolithography, combined with Argon ion-beam etching (IBE) has emerged as the most widely used technique for patterning YBCO SQUIDs and input circuits. Sometimes special masks are used if edge definition is crucial, as e.g., for the fabrication of step-edge and ramp-edge junctions (see section 4) and for patterning submicrometer structures [35,26]. To minimize damage to the YBCO, one restricts the beam energy and current density to below 500 eV and 1 mA/cm^2, respectively. Oxygen loss of the film due to excessive heating can be avoided by using a water or liquid nitrogen cooled sample stage. The impact of ion-beam voltage, current density and sample cooling on the critical current density in narrow linewidth structures has been studied systematically [37], and it has been shown that for high-quality, c-axis YBCO films, the edges are damaged over a length of much less than 1 μm. Reactive ion etching (RIE), a standard technique used for patterning semiconductor or LTS thin films, has basic advantages, as high etching rates and large selectivity, which may improve edge definition. Unfortunately, such a process has not yet been shown to work successfully for HTS thin film patterning [37].

3.3. Multilayer Processing

The fabrication of proper input circuits for SQUIDs requires subsequent deposition and photolithographic

patterning of various superconducting and insulating layers to form superconducting interconnects (vias) and crossovers. Key requirements are epitaxial growth throughout all layers, particularly over patterned edges and full oxygenation of the lower films.

Following the pioneering work by Kingston et al. [38] many groups developed such a technology for HTS thin films, initially using shadow masks and later on photolithographic processing with chemical wet etching or ion beam etching Although integrated integrated magnetometers with up to 15 epitaxial layers have been made [39], it is difficult to maintain high crystalline quality throughout so many layers as is required for high yield and low levels of 1/*f* noise. Thus, most work has been confined to trilayers based on YBCO/insulator/YBCO films. The most widely used insulator is STO. As an alternative to insulating materials, $PrBa_2Cu_3O_{7-\delta}$ (PBCO) has been used in the fabrication of multiturn flux transformers [40].

Standard characterization of multilayer structures includes electrical transport measurements of T_c and j_c of all YBCO layers and of vias and crossovers, as well as measuring the resistivity across the insulating film. Quite early, operation of the basic components at 77 K has been demonstrated, including working flux transformers. However, progress in performance of Josephson junctions and low noise dc SQUIDs made evident that 1/*f* noise in multilayer structures is a key issue [41], which in fact limited the performance of most multilayer devices until today.

Subsequently, improved processes were developed to fabricate most of the low-noise multilayer magnetometers mentioned in section 5. Each layer is usually patterned with Argon IBE at a high angle of incidence to obtain gently sloped edges on the lower layers, essential for the epitaxial growth of subsequent layers. Protection of the surface of the lower YBCO film against degradation from photoresist is achieved by deposition of an *in-situ* STO layer (cap layer). Alternatively, a brief Ar ion beam etch has been used to clean the surfaces before the deposition of the next layer. The improved integrity of the insulator however inhibits the necessary oxygen diffusion and sufficient oxygenation of the lower YBCO film, which results in reduced T_c. Hence, re-oxygenation of the lower YBCO film requires either annealing in an oxygen plasma rather than in molecular O_2, or a considerable increase in the annealing time. With the improved process described above, critical current densities up to $3 \times 10^6\,\mathrm{Acm}^{-2}$ for crossovers [42] and above $1 \times 10^6\,\mathrm{Acm}^{-2}$ for vias [40,43] have been achieved at 77 K. For more details on HTS multilayer processing see [5] and references therein.

3.4. 1/f Noise in YBCO Films

The main requirement for YBCO films used in SQUIDs is a low level of magnetic flux noise generated by vortex motion. Therefore, optimization of the deposition processes described above requires detailed knowledge of the flux noise generated in each superconducting layer. Measurements of the critical current density j_c give only limited information on pinning energies since they are performed with strong driving forces applied by currents and since only the crossection of the smallest critical current in a test structure is detected.

In contrast, flux noise measurements performed in weak magnetic fields (below 10^{-4}T) probe directly pinning energies. This kind of measurements have been pioneered by Ferrari et al. [44–47], who studied the flux noise in high-T_c thin films and single crystals (at variable temperature) by measuring their fluctuating magnetization with a sensitive LTS dc SQUID operated at 4.2 K. From this work it is known that 1/*f* flux noise decreases dramatically with improved crystalline quality of YBCO films. For example, for a polycrystalline YBCO film a flux noise power of $3 \times 10^{-4}\Phi_0^2/\mathrm{Hz}$ at 1 Hz and 40 K was found [44], whereas values below $10^{-10}\Phi_0^2/\mathrm{Hz}$ at 1 Hz and 77 K were obtained for high-quality epitaxial YBCO films [48].

Subsequently, the availability of HTS dc SQUIDs with low levels of 1/*f* noise allowed the measurement of the flux noise of HTS films in LN_2 more straightforwardly by mounting them directly on such a SQUID [42,49,50]. This kind of measurements provided important feedback for optimization of a low noise HTS multilayer technology and resulted in improved low frequency performance of HTS multilayer magnetometers [51].

4. Josephson Junctions

The reliable fabrication of Josephson junctions with reproducible parameters is essential for the fabrication and optimization of sensitive SQUIDs. Unfortunately, in contrast to the $Nb/Al_2O_3/Nb$ trilayer technology for LTS junctions [52], such a HTS technology does not

yet exist. Major problems are created by the requirement for epitaxial growth, which limits the choice of materials and processing techniques. Second, in contrast to Nb, the superconducting coherence length ξ in HTS materials is both short and highly anisotropic, typically 2 nm in the ab-plane and 0.2 nm in the c-axis direction. Hence the properties of high-T_c materials depend strongly on structural and chemical changes *on atomic length scales*. A strong reduction of the I_0R product due to the suppression of the superconducting order parameter at the superconductor-barrier interface can only be avoided if the superconducting electrodes have perfect crystallinity, and if a well-defined interface can be obtained within a single unit cell. Third, it is extremely difficult to fabricate a well-defined barrier with high crystalline quality and homogeneity. Many of the possible barrier materials like PBCO are oxides close to a metal-insulator transition with complex crystal structure and a strong sensitivity to defects on an atomic length scale. As a result transport across these barriers is highly dependent on microstructural imperfections in the barrier and at the interface with the electrodes.

A wide variety of HTS Josephson junctions have been used to fabricate SQUIDs. They fall into three different classes [53]: junctions with intrinsic interfaces (grain boundaries), extrinsic interfaces (extrinsic barriers) and without interfaces (weakened structures). For more details and references on fabrication and properties of HTS Josephson junctions see [5,53,54].

4.1. Grain Boundary Junctions

This new class of Josephson junctions has no analog in low-T_c superconductors. It is based on the strong anisotropy of the high-T_c cuprates and involves weak coupling between two superconducting grains with different orientations, in the so-called grain boundary junctions (GBJs) [55,56]. In fact, the first HTS dc SQUIDs were fabricated with naturally occuring grain boundaries in polycrystalline YBCO films [57]. Subsequently, three types of engineered GBJs were developed: bicrystal, step-edge and bi-epitaxial GBJs [Fig. 4(a)–(c)].

4.1.1. Bicrystal Grain Boundary Junctions. The development of a useful high-T_c Josephson junction technology and the understanding of transport across

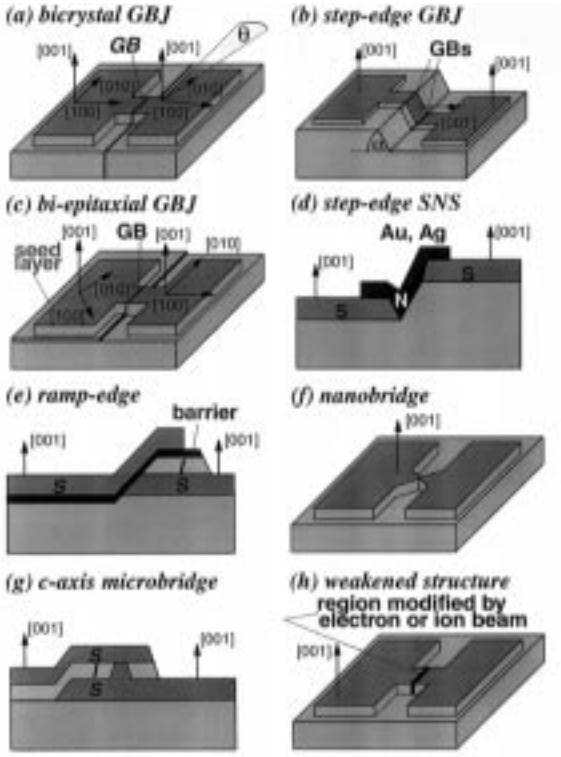

Fig. 4. Schematic view of various types of HTS Josephson junctions.

grain boundaries was pioneered by the work on bicrystal GBJs at IBM, Yorktown Heights [58]. A bicrystal GBJ is fabricated by the epitaxial growth of a high-T_c thin film on a bicrystal substrate with a predetermined misorientation angle θ [Fig. 4(a)]. In contrast to other GBJ fabrication techniques (see below), this method can be used to obtain arbitrary misorientation angles and geometries [59], enabling a systematic study of transport across high-T_c grain boundaries. The grain boundary is formed along a straight line running across the substrate. Hence, this technique is appropriate for SQUIDs or for other applications which do not require many junctions at arbitrary position on a chip. Given a well defined grain boundary in a bicrystal substrate, the fabrication technology for this junction type is the most reliable and successful currently available.

Bicrystal junctions exhibit characteristics close to the RSJ-model provided θ exceeds a critical value, about 10° for YBCO [59,55]. The critical current density j_c for YBCO junctions decreases exponentially with increasing θ [60,61]. This behavior has been explained with an increase of the barrier

thickness with increasing θ. Particularly at large misorientation angles (approaching 45°) the faceting of the grain boundary combined with d-wave pairing symmetry is expected to give a further contribution to the suppression of j_c with θ [62]. For fixed θ, the critical current density can be changed by more than one order of magnitude by appropriate annealing in oxygen [63], implying that the barrier thickness or height depends on oxygen content. Most SQUIDs have been made from YBCO films on 24° or 36° STO bicrystals. With $\theta = 24°$ their I_0R product is typically $0.1 - 0.3$ mV at 77 K, corresponding to $j_c \approx 10^4$A/cm^2. Although standard deviations in j_c and I_0R of around 20% have been reported for junctions on a given bicrystal [41,64], the parameters often vary much more widely because of variations in the quality of the bicrystal substrate.

4.1.2. Step-edge Grain Boundary Junctions. If an epitaxial c-axis YBCO film is grown over a steep step in the substrate or deposited film it changes its orientation at the step, which results in the formation of at least two grain boundaries at the lower and upper edge of the step [Fig. 4(b)]. After this technique had been introduced [65] it was subsequently refined by several groups and is now used for fabrication of practical devices. Common substrate materials are STO and $LaAlO_3$. For large step angles ($\alpha > 70°$) the weak link behavior is determined solely by the lower grain boundary [66]. The substrate steps are usually patterned by lithography and Ar ion milling. Hence, their location can be chosen at will, which gives more freedom in circuit design as compared to the bicrystal technique. However, the properties of step-edge junctions depend strongly on the microstructure of the milled step and on the film growth conditions. Therefore a well controlled edge definition and film growth is essential for this process. Similarly to the bicrystal GBJs, it is possible to trim the junction parameters by an appropriate annealing process [67]. I_0R products are similar to those obtained with bicrystal GBJs.

4.1.3. Bi-epitaxial Grain Boundary Junctions. The 45° in-plane rotation of an epitaxially grown MgO-film on r-plane Sapphire or of a $CeO_2 -$ film on STO has been used to fabricate asymmetric 45° GBJs with a photographically defined grain boundary [68]. The structure consists of a patterned seed layer and a buffer layer on top of which the HTS film is deposited [Fig. 4(c); buffer layer not shown]. The absence of topological limitations and the freedom to design grain boundaries of arbitrary shape and at arbitrary locations are appealing. However, the large misorientation angle results in very low I_0R products, and the spread in the parameters is high, most likely due to inhomogeneities and defects introduced by the edge definition of the seed layer.

4.2. Extrinsic Barrier Junctions

This class of junctions involves a thin deposited interlayer between two superconducting electrodes. Hence extrinsic interfaces are involved, and the control of their properties requires an advanced fabrication technology.

4.2.1. Step-edge-SNS Junctions. The step-edge SNS junction [Fig. 4(d)] is fabricated by cutting a steep step in the substrate, using photolithography and Ar ion milling [69]. Directional deposition of a high-T_c film leads to formation of a gap at the step. This is filled *in-situ* by directional deposition of Au or Ag, making contact to the *a-b* planes of the high-T_c films. Very high I_0R products, up to 1 mV at 77 K, and high normal resistance, above 10Ω for 4–8 μm width, have been reported. However quite often the IVCs show significant deviations from the RSJ-model, and transport and noise properties are still unsettled issues. The major problem appears to be the lack of control of the interface properties which determine R and are most likely responsible for the large spreads in I_0. These difficulties have hindered the application of this type of junction to SQUIDs.

4.2.2. Ramp-edge Josephson Junctions. Ramp-edge junctions [Fig. 4(e)] require the fabrication of an epitaxial trilayer with two superconducting electrodes separated by a thin barrier layer [70]. Current transport is along the *a-b* planes of the *c*-axis oriented electrode films, taking advantage of the larger coherence length along this direction. Fabrication starts with deposition of a insulator-on-YBCO bi-layer, which is patterned to form a ramp with a shallow angle (typically 10° to 20°) using ion milling or anisotropic wet etching. Finally, the barrier material, (e.g., doped YBCO, PBCO or STO) and top electrode are deposited *in-situ*. A key requirement is the fabrication of a lower electrode with a smooth ramp-edge of excellent crystalline quality to support

the growth of a thin, homogenous barrier. Thus, any damage caused by milling the ramp or by its exposure to air has to be healed prior to deposition of the barrier. Alternatively to the deposition of a thin barrier, the surface of the ramp can be modified by ion milling or an in-situ plasma treatment, which leads to formation of a thin layer of a non-superconducting phase of YBCO [71].

The transport mechanism can be of various types, like proximity effect coupling for junctions with low or negligible interface resistance, or transport via tunneling through localized states in the barrier or interface. Quasi-planar junctions with PBC(Ga)O barriers that exhibited negligible interface resistance have been fabricated using bromine etching [72]. IVCs of these junctions were close to the RSJ-model with $I_0R \sim 200\,\mathrm{mV}$ and $\mathrm{R} \sim 1\Omega$ at 77 K, which is appropriate for SQUIDs.

4.3. Weak Links

This class of junctions [Fig. 4(f)–(h)] involves either a narrow constriction, such as a planar nanobridge or a *c*-axis microbridge, or a weakened structure, in which the superconducting properties of a thin film are locally degraded after its deposition. These junction types generally show much larger deviations from the RSJ-behavior than the ones discussed above, and transport and noise properties are not very well understood. Although SQUID operation has been presented with most of these junctions, only the weak links created by oxygen ion irradiation [73] were used to fabricate practical devices; but no systematic data on transport and noise have been reported. Therefore this class of junctions will not be discussed here in more detail.

To conclude this section on junctions, it should be noted that many high-T_c junctions show RSJ-like IVCs, however significant deviations are frequently observed. Furthermore GBJs and junctions with artificial barriers show a scaling $I_0R \propto j_c^p$ $(p \approx 0.5)$ over seven orders of magnitude in j_c, and fluctuations in I_0 and R induce large levels of $1/f$ noise in most junction types [53]. The universal scaling of I_0R is probably the most important feature of high-T_c junctions because it may be the key to understanding their transport and noise properties and offers the possibility of adjusting important junction parameters for optimum SQUID performance. The fact that both GBJs and junctions with artificial barriers have the same scaling suggests a common transport mechanism governed by thin interface layers. However, the details of this mechanism are still controversial [5,53].

5. Practical Devices

5.1. Practical dc SQUIDs

Most dc SQUIDs are fabricated in a square washer design, which allows coupling to a flux transformer, to form a magnetometer or gradiometer. A selection of washer designs on bicrystal substrates made at UC Berkeley is shown in Fig. 5. The designs differ in the location of the Josephson junctions which modifies the SQUID inductance and the effective area [74]. For a typical outer dimension of 500 μm and $L = 40\,\mathrm{pH}$, the type A/C gives the largest A_{eff}. However, the grain boundary line intersects most of the washer, which can induce large $1/f$ noise due to vortex motion along this line, particularly if the device is cooled in the ambient magnetic field.

In most cases the SQUIDs are immersed in LN_2, and to measure their intrinsic noise they are surrounded by magnetic shields to greatly attenuate the ambient field. Additionally HTS shields have been used to provide even greater attenuation of time-varying fields. For almost all applications the SQUIDs are operated in a flux-locked loop (FLL), in which the voltage change across the SQUID induced by an applied flux is amplified and fed back as an opposing flux. The FLL linearizes the SQUID response, provides a straightforward means of measuring the intrinsic SQUID noise, and allows to track inputs equivalent to many flux quanta. Due to large I_0-fluctuations of almost all types of HTS Josephson junctions, it is essential to use appropriate electronic read-out schemes (bias reversal) to cancel their contribution to $1/f$ noise. For details on readout schemes see [5,28].

Very low levels of rms flux noise $S_\Phi^{1/2} \simeq 1.4\mu\Phi_0 Hz^{-1/2}$ and energy resolution $\varepsilon \simeq 2 \times 10^{-31}\,\mathrm{J/Hz}$ have been achieved at 77 K in the white noise limit [75–77]. More typical values are a few $\mu\Phi_0\mathrm{Hz}^{-1/2}$ and $10^{-30}\,\mathrm{J/Hz}$ which extend down to about 1 Hz if the SQUIDs are operated with bias reversal. A typical noise spectrum for a YBCO bicrystal dc SQUID is shown in Fig. 6. Except for a few cases [77] the experimental values for ε are

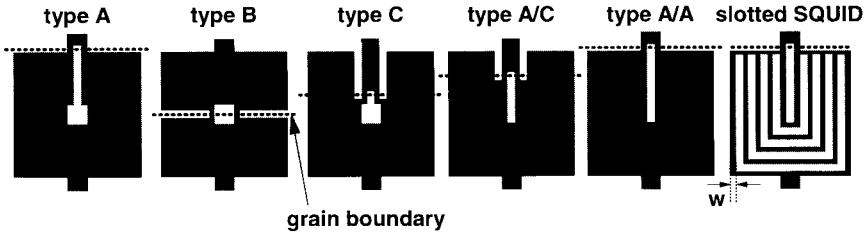

Fig. 5. Design of dc SQUID washers.

typically an order of magnitude above the theoretical predictions [5], which is not yet understood. However this sensitivity is still very adequate for applications if it can be maintained for SQUIDs coupled to proper input circuits.

The $1/f$ noise power in unpatterned films and in washer SQUIDs increases linearly with cooling field, due to the penetration of vortices during cooling through T_c [47,78]. Therefore it is essential that for operation of SQUIDs in unshielded environment one either effectively pins the flux vortices or eliminates their presence in the film. The latter approach has been taken by Dantsker et al. [79,80], who fabricated slotted SQUIDs as the one shown in Fig. 5. For a film of width w cooled in a perpendicular field B_0, penetration of vortices is energetically unfavorable if $w \leq (\pi\Phi_0/4B_0)^{1/2}$ [81]. For a slotted SQUID with $w = 4\,\mu$m the $1/f$ noise at 1 Hz started to increase for a cooling field around $130\,\mu$T, which is roughly a factor of two above the earth magnetic field. Large changes in magnetic field while the SQUIDs are operated below T_c, e.g., if the SQUIDs are rotated in the ambient magnetic field, can also induce a significant increase in low frequency noise and hysteresis [5].

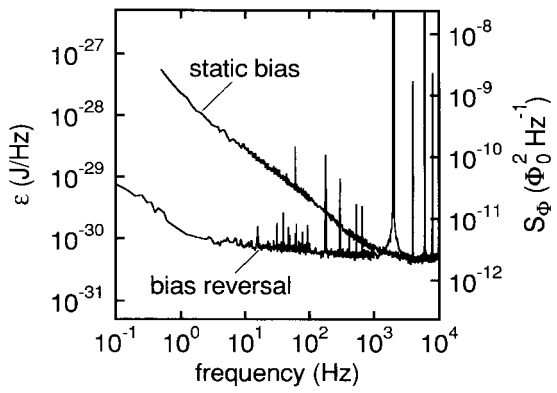

Fig. 6. Energy resolution and spectral density of flux noise of a bicrystal dc SQUID operated at 77 K with flux modulation and bias reversal [5].

For 500 μm washer SQUIDs, A_{eff} is on the order of $10^{-8}\,\mathrm{m}^2$. As a consequence, a flux noise of a few $\mu\Phi_0\mathrm{Hz}^{-1/2}$ corresponds to a magnetic field resolution around $1\,\mathrm{pT\,Hz}^{-1/2}$, which is not adequate for many applications. Various schemes for improvement of S_B, as discussed in section 2.3.1 have been realized. A selection of devices is shown in Fig. 7.

Directly-coupled magnetometers based on YBCO dc SQUIDs with bicrystal GBJs [Fig. 7(a)] have been the first devices which achieved magnetic field resolutions below $100\,\mathrm{fTHz}^{-1/2}$ at frequencies as low as 1 Hz and $T = 77$ K [82]. Subsequent optimization of the SQUID parameters and reduction of the large mismatch between L_p and L lead to $S_B^{1/2} \approx (20\text{–}40)\mathrm{fTHz}^{-1/2}$ in the white noise limit for devices on $1\,\mathrm{cm}^2$ substrates [83–85]. At $f = 1$ Hz the noise increased slightly to about $(60\text{–}70)\mathrm{fTHz}^{-1/2}$ if the SQUIDs were operated with bias reversal. This simple single layer approach, which adds only small or negligible excess low frequency noise (at 1 Hz), has also been extended to the use of single layer flux transformers. Such a transformer consists of a very large pickup loop and a single turn input coil, which is coupled to the pickup loop of a directly-coupled magnetometer in a flip chip arrangement. With a transformer fabricated on a 2 inch waver $S_B^{1/2}(1\mathrm{Hz}) = 39\mathrm{fTHz}^{-1/2}$ has been achieved [49]. Furthermore, the direct coupling scheme offers the advantage to easily implement narrow linewidth SQUIDs. In principle, cooling such devices in the ambient magnetic field should not add significant excess low frequency noise. This makes this single layer magnetometer approach quite appealing, particularly for geophysical applications, where magnetic shielding is not possible, but large pickup areas can be tolerated.

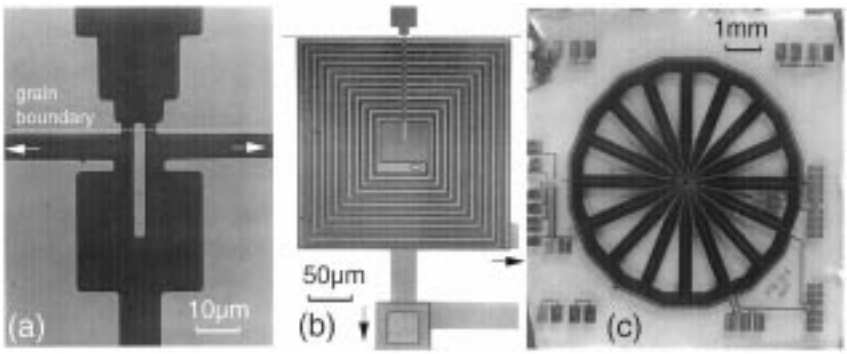

Fig. 7. Photographs of dc SQUID magnetometers made at UC Berkeley: (a) 20 pH washer SQUID—part of directly-coupled magnetometer; (b) washer SQUID (bottom layer) with spiral input coil (upper layer) integrated on the same chip; (c) multiloop SQUID [87]. Arrows indicate connection to pickup loop.

The coupling of input signals to a SQUID is efficiently improved if a flux transformer with a multiturn input coil is used. Effective areas of such HTS devices on 1 cm^2 chips are around (1–2)mm^2, which is an order of magnitude above A_{eff} for typical direct coupled magnetometers. The first flip-chip magnetometer with a low noise bicrystal dc SQUID achieved a magnetic field resolution below 40 $fTHz^{-1/2}$ in the white noise limit. However large excess $1/f$ noise from the flux transformer deteriorated its performance strongly to a level of 1.7 $pT\,Hz^{-1/2}$ at 1 Hz [41]. Subsequently the refinement of the HTS multilayer technology lead to a dramatic improvement in the low frequency performance of this type of magnetometers. Together with further optimization of the performance of bare SQUIDs and of the inductive coupling between transformer and SQUID this lead to low levels of magnetic field noise at 77 K: 8.5 $fTHz^{-1/2}$ in the white noise limit and 27 $fTHz^{-1/2}$ at 1 Hz [51], for the best device reported so far. Integration of SQUID and flux transformer on the same chip [Fig. 7(b)] has also been achieved with a similarly low level of magnetic field noise in the white noise limit [86]. The integration of SQUID and flux transformer may eventually lead to improved coupling, however up to now there is no clear experimental evidence for this assumption [50]. Apart from frequently observed resonances in these structures, which have not been reported for flip chip magnetometers, and which are well known from LTS magnetometers to degrade the SQUID performance [20], a major drawback of integrated HTS magnetometers is the low yield of fabricating high performance devices. This also holds for the other type of integrated magnetometer, the multiloop SQUID [Fig. 7(c)]. A device based on bicrystal GBJs with 16 loops in parallel, with an outer diameter of 7 mm had an estimated inductance of 145 pH and an effective area of 1.9 mm^2. Despite its relatively large inductance, the almost optimum junction parameters for this device lead to a low level of white flux noise and a magnetic field resolution of 18 $fTHz^{-1/2}$ at 1 kHz and 37 $fTHz^{-1/2}$ at 1 Hz [87].

5.2. *Practical rf SQUIDs*

During the past few years the performance of HTS rf SQUIDs improved impressively (for details see Ref. [5] and references therein). Major contributions to this field were made by the group at the Forschungszentrum (FZ) Jülich, who replaced the standard design of the tank circuits, based on lumped elements, by high Q microwave resonator structures. This step allowed an increase of the rf pump frequency up to about 1 GHz, with a concomitant increase in transfer function and reduction in flux noise. Similarly to dc SQUIDs, the rf SQUIDs are also operated in a FLL. Most devices operate in the non-hysteretic mode and are based on single layer, large washer rf SQUIDs [see Fig. 3(a)] with step-edge GBJs. The SQUID inductance is typically within 100–300 pH, which is much higher than for optimized dc SQUIDs. The junction parameters are usually trimmed until $\tilde{\beta}_L \approx 1$, which results in very small critical currents. Although not known precisely, it is expected that Γ is close to unity. Hence, these devices are operated in the limit of large thermal fluctuations, which is described by the theory of Chesca [21].

In one of the most recent designs a large washer SQUID (typically 3 mm in diameter) is inductively coupled to a thin film flux concentrator, surrounded by a coplanar resonator [Fig. 8(a)]. A 260 pH SQUID coupled to such a resonator with a 13 mm-diameter flux concentrator had a white rms flux noise of $8.5\mu\Phi_0 Hz^{-1/2}$, corresponding to an energy resolution of 6×10^{-31} J/Hz and magnetic field resolution of $16\,fTHz^{-1/2}$ at a pump frequency of 650 MHz and $T = 77$ K [88]. The noise at 1 Hz however was substantially higher, about $100\,fTHz^{-1/2}$, most likely due to vortex motion in the washer or flux concentrator. An important step towards even better sensitivity involves the use of a multilayer flux transformer [Fig. 8(b)]. This design integrates a planar superconducting flux transformer and a planar resonator on one chip. The flux transformer consists of the outer rectangular pickup loop and a multiturn input coil, similarly to flux transformers used for dc SQUIDs. The transformer couples the low frequency signal to one half of a two-hole rf SQUID [Fig. 8(c)]. Inside the pickup loop, separated by an rf shielding ring, a labyrinth resonator couples the rf signal to the second half of the two-hole SQUID via a single turn rf input coil. The separation between low-frequency and rf currents allows to maintain a high Q factor. For a device fabricated on a 1 cm^2 substrate and coupled to a two-hole rf SQUID in a flip-chip arrangement, a magnetic field noise of $11\,fTHz^{-1/2}$ has been achieved in the white noise limit [89]. However, the low frequency noise of this device was substantial and most likely arose from vortex motion in the flux transformer.

5.3. Practical Gradiometers

Various gradiometer configurations have been realized with HTS SQUIDs. These include axial gradiometers, based on large washer rf SQUIDs with electronic subtraction and planar, off-diagonal gradiometers based on both, multilayer and single layer devices. The latter used either large washer two-hole SQUIDs or the direct-coupling scheme and were sometimes coupled to large single layer gradiometric flux transformers to increase their baseline. Due to the short baseline of the planar off-diagonal gradiometers, their gradient sensitivity may not be adequate for biomagnetic applications, however they have been shown to be useful for applications in nondestructive testing (section 6.2). For more details and references see [5]

6. Applications

The steady improvement in sensitivity of HTS SQUIDs opened up a wide field of possible applications. In most cases the bare sensors, or HTS SQUIDs integrated in prototype systems have been used to demonstrate their feasibility for various applications.

6.1. Biomagnetism

Biomagnetic applications of SQUIDs have been focused on magnetoencephalography (MEG) and magnetocardiology (MCG) to detect signals from

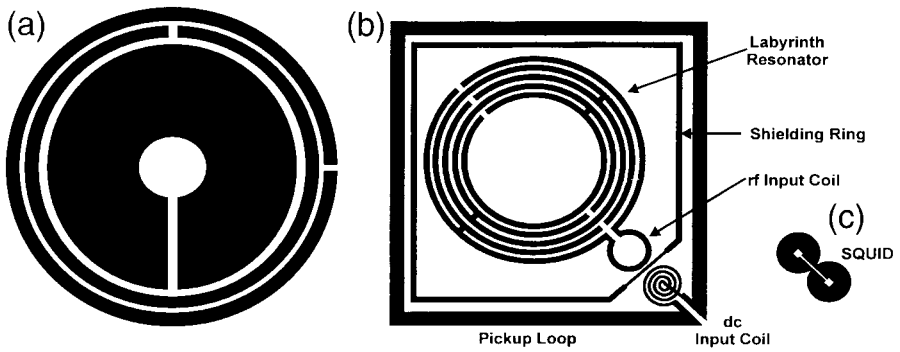

Fig. 8. Layouts for input coupling to rf SQUIDs: (a) flux concentrator with coplanar resonator [88]; (b) flux transformer for two-hole rf SQUID and (c) two hole rf SQUID [89].

the human brain and heart, respectively. MEG demands a magnetic field resolution of a few $fTHz^{-1/2}$ at frequencies down to about 1 Hz. Most commercial LTS SQUIDs are used in multichannel systems for this application; some of them with more than 100 channels. Although neuromagnetic measurements, e.g., of signals from the central and peripheral nervous system with 100 fT amplitudes [86,90] have been demonstrated with HTS SQUIDs, their sensitivity appears not yet to be sufficient for most applications in MEG. On the other hand, MCG requires typically field resolutions of some tens of $fTHz^{-1/2}$ in the same frequency range. Therefore most biomagnetic measurements with HTS SQUIDs focused on this application.

Figure 9 shows a real-time trace of an MCG measured in a magnetically shielded room with the most sensitive integrated HTS dc SQUID magnetometer ($S_B^{1/2}(1\text{kHz}) = 10\,\text{fTHz-1/2}$ and $53\,fTHz^{-1/2}$ at 1 Hz) [86] fabricated to date. The signal-to-noise ratio of 130 for the R-peak is acceptable for low-T_c MCG systems. An important point is that HTS devices may be somewhat less sensitive than LTS devices since they gain in signal-to-noise ratio due to the possible operation at a smaller source-to-sensor distance [91]. Multichannel systems which allow spatial field mapping have also been fabricated with HTS SQUIDs, with up to 32 sensors [92]. However the magnetic field resolution of their large washer SQUIDs was about an order of magnitude above the values required for useful MCGs.

The advantage of relaxed cryogenic requirements for HTS SQUID systems will probably not result into significantly reduced costs of a MEG system, unless the expensive magnetic shielding can be avoided. Although 2nd order electronic gradiometers have been used to record good quality MCG without shielding [93], unshielded multi-channel systems still operate at noise levels clearly above $100\,fTHz^{-1/2}$. However, significant progress in this field is still possible.

6.2. *Nondestructive Evaluation*

Nondestructive evaluation (NDE) is an important technique for materials inspection in highly safety relevant areas, such as testing of aircraft components, or reinforcing rods in concrete structures. The requirement for magnetic field resolution is clearly relaxed as compared to biomagnetic applications. Furthermore, LN_2 cooling allows fabrication of smaller and less expensive systems as compared to LHe cooling, and even commercial cryocoolers have been successfully employed in HTS systems for NDE applications [94,95].

In *eddy-current imaging*, a widely used technique to detect subsurface cracks in metallic structures [96], the perturbation of field induced eddy currents by structural defects causes a distortion of the magnetic field to be measured. Detection of deep lying defects requires low frequency operation. Hence, the high dynamic range and the flat frequency response of SQUID systems leads to a significant advantage over conventionally used induction coils. Eddy current detection with HTS rf SQUIDs has been successfully demonstrated in an aircraft hangar to detect cracks in aircraft felloes [97,98], as shown in Fig. 10. The

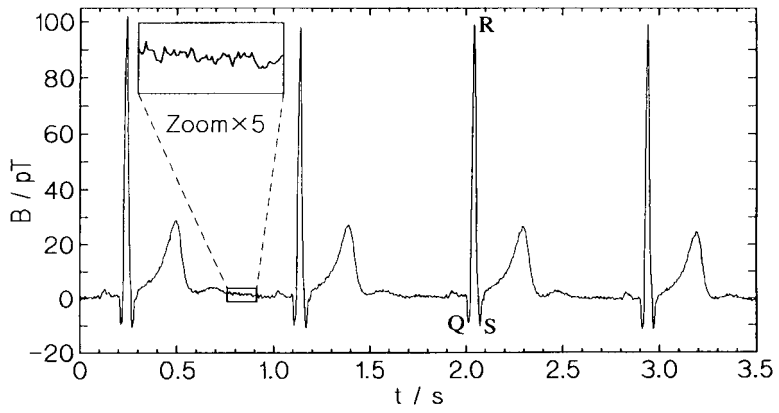

Fig. 9. Real-time trace of magnetocardiogram recorded with integrated HTS dc SQUID magnetometer in a magnetically shielded room (bandwidth: 0.016–200 Hz; no power line filters) [86].

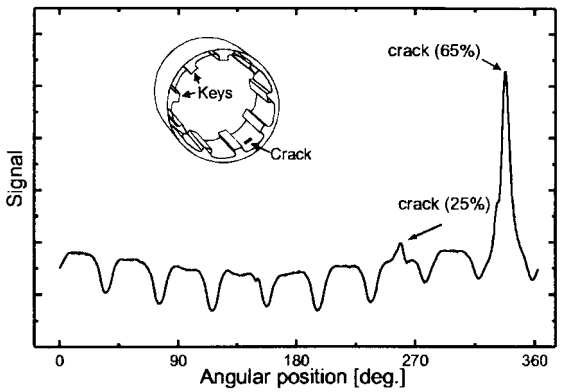

Fig. 10. SQUID signal track recorded in one rotation of Airbus wheel with artificial inner flaws [98].

periodic structure is in part due to the presence of the ferromagnetic steel bars (keys). The signals from cracks, which penetrate 25% and 65% of the wall thickness are clearly visible. The smaller crack lies beyond the detection limit of conventional low frequency eddy current devices.

Another SQUID NDE technique is based on the detection of magnetic fields generated by magnetized particles or components in the devices under test. An important HTS SQUID application of this type has been already established on the NDE market: Using a second order electronic rf SQUID gradiometer [93], ferrous inclusions in disks of turbine engine rotors are detected [99]. If the density of such inclusions induced by the manufacturing process exceeds a critical value, they can lead to failure of the aircraft engine.

6.3. *Scanning SQUID Microscopy*

The combination of high sensitivity to magnetic flux or field and high spatial resolution is combined in scanning SQUID microscopy. HTS SQUID microscopes have been built for imaging at 77 K or at room temperature [100,101]. The spatial resolution is given by the size of the pickup structure, typically on the order of 10 μm or by the SQUID-to-sample distance, as small as a few μm for cooled samples and typically on the order of 50–100 μ for warm samples. These systems have been applied to eddy current microscopy ($f = 1$ kHz–1 MHz) [102], rf microscopy ($f = 1$ MHz–1 GHz) and microwave microscopy above 1 GHz [103]. For one system a SQUID-to-sample distance as low as 15 μm has been achieved with a 3 μm thin Si_xNi_y window, separating the sample at room temperature from the SQUID which is placed on a cold finger in vacuum [101]. A novel application of this microscope, in which the sample is held fixed, is the detection of flux noise from the motion of magnetotactic bacteria with a magnetic moment of about 5×10^{-16}Acm^2 for a single bacterium. Possible measurements include the dynamics of living bacteria [104], the effects of an applied magnetic field, and the migration of bacteria through porous media.

6.4. *Geophysics*

Liquid Helium cooled SQUIDs have been demonstrated to be useful for a variety of geophysical applications, like magnetotellurics (MT), controlled source electromagnetics (CSEM) or transient electromagnetics (TEM) and cross-borehole sounding [105]. The introduction of LN_2 cooled SQUIDs is expected to have a major impact on geophysical SQUID applications, due to the possible reduction in system size and significant increase in cryogenic hold time, which is of great importance for operation in remote areas. Most applications require the use of an orthogonal set of three magnetometers. A HTS version of such a 3-axis magnetometer has been built with directly-coupled dc SQUID magnetometers and was operated with sufficient slew rate for use in the ambient field [106]. A German consortium developed 3-axis HTS rf SQUID magnetometers for TEM and showed its applicability in various field tests [107,108]. The comparison with a commercial induction coil system showed a superior signal-to-noise ratio for the HTS SQUID system. If such unshielded systems achieve low levels of magnetic field resolution, on the order of some ten fTHz$^{-1/2}$ down to low frequencies, possibly below 1 Hz, they are expected to be very competitive with the conventional induction coil technique.

7. Conclusions

The progress in HTS thin film and Josephson junction technology resulted in the demonstration of greatly improved performance of YBCO SQUIDs and SQUID based devices at a level which is already quite adequate for some real-world applications. However, a major problem, which still has to be

solved, is the lack of a more reliable and reproducible process for low noise thin film multilayer structures and for well defined Josephson junctions. This probably requires a much deeper understanding of the complex interplay between processing parameters, thin film microstructure and transport and noise properties. On the other hand, much work still has to be done to integrate HTS SQUIDs into systems useful for applications and to demonstrate adequate performance if the SQUIDs are operated in unshielded or only moderately shield environment. Avoiding expensive magnetic shielding will allow to take advantage of the relaxed cryogenic requirements for LN_2-cooled SQUIDs, and this may eventually lead to much more widespread applications of these devices.

Acknowledgments

I wish to thank John Clarke, Reinhold Kleiner, Frank Ludwig and Gene Dantsker for fruitful collaboration and Achim Marx for his support during preparation of this review.

References

1. J.G. Bednorz and K.A. Müller, *Z. Phys. B*, **64**, 189 (1986).
2. B.D. Josephson, *Phys. Lett*., **1**, 251 (1962).
3. B.D. Josephson, *Adv. Phys*., **14**, 419 (1965).
4. H. Weinstock, Ed., *SQUID Sensors: Fundamentals, Fabrication and Applications* (Kluwer Academic Publishers, Dordrecht), (1996).
5. D. Koelle, R. Kleiner, F. Ludwig, E. Dantsker, and J. Clarke, *Rev. Mod. Phys*., **71**, (April, 1999).
6. B.S. Deaver and W.M. Fairbank, *Phys. Rev. Lett*., **7**, 43, (1961).
7. R. Doll and M. Näbauer, *Phys. Rev. Lett*., **7**, 51, (1961).
8. R.C. Jaklevic, J. Lambe, A.H. Silver, and J.E. Mercereau, *Phys. Rev. Lett*., **12**, 159 (1964).
9. W.C. Stewart, *Appl. Phys. Lett*., **12**, 277 (1968).
10. D.E. McCumber, *J. Appl. Phys*., **39**, 3113 (1968).
11. C.D. Tesche and J. Clarke, *J. Low Temp. Phys*., **29**, 301 (1977).
12. R. Kleiner, 1996 unpublished; see also Ref. 5.
13. K. Enpuku, H. Doi, G. Tokita, and T. Maruo, *IEEE Trans. Appl. Supercond*., **5**, 2762 (1995).
14. K. Enpuku, G. Tokita, T. Maruo, and T. Minotani, *J. Appl. Phys*., **78**, 3498 (1995).
15. B. Chesca, *J. Low Temp. Phys*., **112**, 165 (1998).
16. B. Chesca, ''The effect of thermal noise on the operation of dc SQUIDs at 77 K—a fundamental analytical approach,'' Applied Superconductivity Conference (ASC'98), Palm Desert, CA; to be published in *IEEE Trans. Appl. Supercond.* **9**, (1999).
17. J.E. Zimmerman, P. Thiene, and J.T. Harding, *J. Appl. Phys*., **41**, 1572 (1970).
18. J.E. Mercereau, *Rev. Phys. Appl*., **5**, 13 (1970).
19. M. Nisenoff, *Rev. Phys. Appl*., **5**, 21 (1970).
20. T. Ryhänen, H. Seppä, R. Ilmoniemi, and J. Knuutila, *J. Low Temp. Phys*., **76**, 287 (1989).
21. B. Chesca, *J. Low Temp. Phys*., **110**, 963 (1998).
22. M.B. Ketchen, *IEEE Trans. Magn*., **17**, 387 (1985).
23. M.B. Ketchen, *IEEE Trans. Magn*., **17**, 387 (1981).
24. J.M. Jaycox and M.B. Ketchen, *IEEE Trans. Magn*., **17**, 400 (1981).
25. J.E. Zimmerman, *J. Appl. Phys*., **42**, 4483 (1971).
26. D. Drung, R. Cantor, M. Peters, H.-J. Scheer, and H. Koch, *Appl. Phys. Lett*., **57**, 406 (1990).
27. D. Drung, R. Cantor, M. Peters, T. Ryhänen, and H. Koch, *IEEE Trans Magn*., **MAG-27**, 3001 (1991).
28. D. Drung, in *SQUID Sensors: Fundamentals, Fabrication and Applications*, NATO ASI Series, edited by H. Weinstock (Kluwer Academic Publishers, Dordrecht), (1996) p. 63 .
29. M.K. Wu, J.R. Ashburn, C.J. Torng, P.H. Hor, R.L. Meng, L. Gao, N.Z. Huang, Y.Q. Wang, and C.W. Chu, *Phys. Rev. Lett*., **58**, 908 (1987).
30. J. Phillips, *J. Appl. Phys*., **79**, 1829 (1996).
31. J. Phillips, in *The New Superconducting Electronics* NATO ASI series, edited by H. Weinstock and R.W. Ralston (Kluwer Academic Publishers, Dordrecht), (1993) p. 59.
32. F.C. Wellstood, J.J. Kingston, and J. Clarke, *J. Appl. Phys*., **75**, 683 (1994).
33. S.E. Russek, S.C. Sanders, A. Roshko, and J.W. Ekin, *Appl. Phys. Lett*., **64**, 3649 (1994).
34. A.I. Braginski, in *The New Superconducting Electronics* NATO ASI series, edited by H. Weinstock and R.W. Ralston (Kluwer Academic Publishers, Dordrecht), (1993) p. 89.
35. J. Schneider, H. Kohlstedt, and R. Wördenweber, *Appl. Phys. Lett*., **63**, 2426 (1993).
36. A.J.M. van der Harg, E. van der Drift, and P. Hadley, *IEEE Trans Appl. Supercond*., **5**, 1448 (1995).
37. L. Alff, G.M. Fischer, R. Gross, F. Kober, A. Beck, K.D. Husemann, T. Nissel, F. Schmidl, and C. Burckhardt, *Physica. C*, **200**, 277 (1992).
38. J.J. Kingston, F.C. Wellstood, P. Lerch, A.H. Miklich, and J. Clarke, *Appl. Phys. Lett*., **56**, 189 (1990).
39. L.P. Lee, K. Char, M.S. Colclough, and G. Zaharchuk, *Appl. Phys. Lett*., **59**, 3051 (1991).
40. M.N. Keene, S.W. Goodyear, J.S. Satchell, J.A. Edwards, N.G. Chew, and R.G. Humphreys, *IEEE Trans. Appl. Supercond*., **3**, 2430 (1993).
41. A.H. Miklich, D. Koelle, E. Dantsker, D.T. Nemeth, J.J. Kingston, R.F. Kroman, and J. Clarke, *IEEE Trans. Appl. Supercond*., **3**, 2434 (1993).
42. F. Ludwig, D. Koelle, E. Dantsker, D.T. Nemeth, A.H. Miklich, J. Clarke, and R.E. Thomson, *Appl. Phys. Lett*., **66**, 373 (1995).
43. M.S. DiIorio, S. Yoshizumi, K.-Y. Yang, M. Maung, J. Zhang, and B. Power, *IEEE Trans Appl. Supercond*., **3**, 2011 (1993).
44. M.J. Ferrari, M. Johnson, F.C. Wellstood, J. Clarke, P.A. Rosenthal, R.H. Hammond, and M.R. Beasley, *Appl. Phys. Lett*., **53**, 695 (1988).

45. M.J. Ferrari, M. Johnson, F.C. Wellstood, J. Clarke, A. Inam, X.D. Wu, L. Nazar, and T. Venkatesan, *Nature*, **341**, 723 (1989).
46. M.J. Ferrari, J.J. Kingston, F.C. Wellstood, and J. Clarke, *Appl. Phys. Lett*., **58**, 1106 (1991).
47. M.J. Ferrari, M. Johnson, F.C. Wellstood, J.J. Kingston, T.J. Shaw, and J. Clarke, *J. Low Temp. Phys*., **94**, 15 (1994).
48. T.J. Shaw, J. Clarke, R.B. van Dover, L.F. Schneemeyer, and A.E. White, *Phys. Rev. B*, **54**, 15411 (1996).
49. D. Koelle, A.H. Miklich, E. Dantsker, F. Ludwig, D.T. Nemeth, J. Clarke, W. Ruby, and K. Char, *Appl. Phys. Lett*., **63**, 3630 (1993).
50. F. Ludwig, E. Dantsker, D. Koelle, R. Kleiner, A.H. Miklich, and J. Clarke, *Appl. Supercond*., **3**, 383 (1995).
51. E. Dantsker, F. Ludwig, R. Kleiner, J. Clarke, M. Teepe, L.P. Lee, N.McN. Alford, and T. Button, *Appl. Phys. Lett*., **67**, 725 (1995).
52. M. Gurvitch, M.A. Washington, and H.A. Huggins, *Appl. Phys. Lett*., **42**, 472 (1983).
53. R. Gross, L. Alff, A. Beck, O.M. Froehlich, D. Koelle, and A. Marx, *IEEE Trans. Appl. Supercond*., **7**, 2929 (1997).
54. A.I. Braginski, in *SQUID Sensors: Fundamentals, Fabrication and Applications* NATO ASI Series, edited by H. Weinstock (Kluwer Academic Publishers, Dordrecht), (1996) p. 235.
55. R. Gross, in *Interfaces in High-Tc Superconducting Systems*, edited by S. L. Shinde and D. A. Rudman (Springer-Verlag, New York), (1994) p. 176.
56. R. Gross, L. Alff, A. Beck, O.M. Froehlich, R. Gerber, R. Gerdemann, A. Marx, B. Mayer, and D. Koelle, *Proc. of the 2nd Workshop on HTS Applications and New Materials* edited by D.H. Blank (University of Twente, The Netherlands), (1995) p. 8.
57. R.H. Koch C.P. Umbach, G.J. Clark, P. Chaudhari, and R.B. Laibowitz, *Appl. Phys. Lett*., **51**, 200 (1987).
58. P. Chaudhari, J. Mannhart, D. Dimos, C.C. Tsuei, C.C. Chi, M.M. Oprysko, and M. Scheuermann, *Phys. Rev. Lett*., **60**, 1653 (1988).
59. D. Dimos, P. Chaudhari, and J. Mannhart, *Phys. Rev. B*, **41**, 4038 (1990).
60. R. Gross, R.P. Chaudhari, M. Kawasaki, and A. Gupta, *IEEE Trans. Magn*., **MAG-27**, 3227 (1991).
61. Z.G. Ivanov, P.Å. Nilsson, D. Winkler, J.A. Alarco, T. Claeson, E.A. Stepantsov, and A. Ya. Tzalenchuk, *Appl. Phys. Lett*., **59**, 3030 (1991).
62. H. Hilgenkamp, J. Mannhart, and B. Mayer, *Phys. Rev. B*, **53**, 14586 (1996).
63. M. Kawasaki, P. Chaudhari, and A. Gupta, *Phys. Rev. Lett*., **68**, 1065 (1992).
64. R. Gerdemann, K.-D. Husemann, R. Gross, L. Alff, A. Beck, and B. Elia, *J. Appl. Phys*., **76**, 8005 (1994).
65. R. Simon, J.B. Bulman, J.F. Burch, S.B. Coons, K.P. Daly, W.D. Dozier, R. Hu, A.E. Lee, J.A. Luine, C.E. Platt, and M.J. Zani, *IEEE Trans. Magn*., **MAG-27**, 3209 (1991).
66. C.L. Jia, B. Kabius, K. Urban, K. Herrmann, J. Schubert, W. Zander, and A.I. Braginski, *Physica. C*, **196**, 211 (1992).
67. F. Dillmann, V.N. Glyantsev, and M. Siegel, *Appl. Phys. Lett*., **69**, 1948 (1996).
68. K. Char, M.S. Colclough, L.P. Lee, and G. Zaharchuk, *Appl. Phys. Lett*., **59**, 2177 (1991).
69. M.S. DiIorio, S. Yoshizumi, K.-Y. Yang, J. Zhang, and M. Maung, *Appl. Phys. Lett*., **58**, 2552 (1991).
70. J. Gao, W.A.M. Aarnink, G.J. Gerritsma, and H. Rogalla, *Physica. C*, **171**, 126 (1990).
71. B.H. Moeckly and K. Char, *Appl. Phys. Lett*., **71**, 2526 (1977).
72. M.I. Faley, U. Poppe, C.L. Jia, U. Dähne, Yu. Goncharov, N. Klein, K. Urban, V.N. Glyantsev, G. Kunkel, and M. Siegel, *IEEE Trans. Appl. Supercond*., **5**, 2091 (1995).
73. S.S. Tinchev, *Supercond. Sci. Technol*., **3**, 500 (1990).
74. F. Ludwig, E. Dantsker, D. Koelle, R. Kleiner, A.H. Miklich, D.T. Nemeth, J. Clarke, D. Drung, J. Knappe, and H. Koch, *IEEE Trans. Appl. Supercond*., **5**, 2919 (1995).
75. M. Kawasaki, P. Chaudhari, T.H. Newman, and A. Gupta, *Appl. Phys. Lett*., **58**, 2555 (1991).
76. R. Cantor, L.P. Lee, M. Teepe, V. Vinetskiy, and J. Longo, *IEEE Trans. Appl. Supercond*., **5**, 2927 (1995).
77. K. Barthel, D. Koelle, B. Chesca, A. Marx, R. Gross, and A.I. Braginski, ''Transferfunction and thermal noise of $YBa_2Cu_3O_7 - \delta$ dc SQUIDs operated under large thermal fluctuations,'' *Appl. Phys. Lett*. **74**, (1999).
78. A.H. Miklich, D. Koelle, T.J. Shaw, F. Ludwig, D.T. Nemeth, E. Dantsker, and J. Clarke, *Appl. Phys. Lett*., **64**, 3494 (1994).
79. E. Dantsker, S. Tanaka, P.-Å. Nilsson, R. Kleiner, and John Clarke, *Appl. Phys. Lett*., **69**, 4099 (1996).
80. E. Dantsker, S. Tanaka, and J. Clarke, *Appl. Phys. Lett*., **70**, 2037 (1997).
81. J. Clem, unpublished (1996).
82. D. Koelle, A.H. Miklich, F. Ludwig, E. Dantsker, D.T. Nemeth, and J. Clarke, *Appl. Phys. Lett*., **63**, 2271 (1993).
83. L.P. Lee, J. Longo, V. Vinetskiy, and R. Cantor, *Appl. Phys. Lett*., **66**, 1539 (1995).
84. V.N. Glyantsev, Y. Tavrin, W. Zander, J. Schubert, and M. Siegel, *Supercond. Sci. Technol*., **9**, A105 (1996).
85. J. Beyer, D. Drung, F. Ludwig, T. Minotani, and K. Enpuku, *Appl. Phys. Lett*., **72**, 203 (1998).
86. D. Drung, F. Ludwig, W. Müller, U. Steinhoff, L. Trahms, Y.Q. Shen, M.B. Jensen, P. Vase, T. Holst, T. Freltoft, and G. Curio, *Appl. Phys. Lett*., **68**, 1421 (1996).
87. F. Ludwig, E. Dantsker, R. Kleiner, D. Koelle, J. Clarke, S. Knappe, D. Drung, H. Koch, N.McN. Alford, and T.W. Button, *Appl. Phys. Lett*., **66**, 1418 (1995).
88. Y. Zhang, N. Wolters, X.H. Zeng, J. Schubert, W. Zander, H. Soltner, M. Banzet, F. Rüders, and A.I. Braginski, to be published in *Appl. Supercond.* (1997).
89. Y. Zhang, H.R. Yi, J. Schubert, W. Zander, H.-J. Krause, H. Bousack and A.I. Braginski ''Operation of rf SQUID Magnetometers with a Multi-Turn Flux Transformer Integrated with a Superconducting Labyrinth Resonator,'' Applied Superconductivity Conference (ASC'98), Palm Desert, CA; to be published in *IEEE Trans. Appl. Supercond*., **9**, (1999).
90. G. Curio, D. Drung, H. Koch, W. Müller, U. Steinhoff, L. Trahms, Y.Q. Shen, P. Vase, and T. Freltoft, *Neurosci. Lett*., **206**, 204 (1996).
91. M. Burghoff, L. Trahms, Y. Zhang, H. Bousack, and J. Borgmann, *J. Clin. Engineering*, **21**, 62 (1996).

92. H. Itozaki, S. Tanaka, H. Toyoda, T. Hirano, Y. Haruta, M. Nomura, T. Saijou, and H. Kado, *Supercond. Sci. Technol.*, **9**, A38 (1996).
93. Y. Tavrin, Y. Zhang, W. Wolf, and A.I. Braginski, *Supercond. Sci. Technol.*, **7**, 265 (1994).
94. R. Hohmann, H.-J. Krause, H. Soltner, Y. Zhang, C.A. Copetti, H. Bousack, and A.I. Braginski, *IEEE Trans. Appl. Supercond.*, **7**, 2860 (1997).
95. M.V. Kreutzbruck, J. Tröll, M. Mück, C. Heiden, and Y. Zhang, *IEEE Trans. Appl. Supercond.*, **7**, 3279 (1997).
96. J.P. Wikswo, *IEEE Trans Appl. Supercond.*, **5**, 74 (1995).
97. M. Mück, M.v. Kreutzbruck, U. Baby, J. Tröll, and C. Heiden, *Physica. C*, **282–287**, 407 (1997).
98. H.-J. Krause, Y. Zhang, R. Hohmann, M. Grüneklee, M.I. Faley, D. Lomparski, M. Maus, H. Bousack, and A.I. Braginski, in *Proceedings of the European Conference on Applied Superconductivity (EUCAS'97) Inst. Phys. Conf. Ser.*, **158**, 775 (1997).
99. Y. Tavrin and J.H. Hinken, ''First Routine Aircraft NDT with a SQUID Gradiometer,'' in *Proceedings of the 7th European Conference on Nondestructive Testing* Kopenhagen, **26–29**, 05 1998.
100. R.C. Black, A. Mathai, F.C. Wellstood, E. Dantsker, A.H. Miklich, D.T. Nemeth, J.J. Kingston, and J. Clarke, *Appl. Phys. Lett.*, **62**, 2128 (1993).
101. T.S. Lee, T.S., Y.R. Chemla, E. Dantsker, and J. Clarke, *IEEE Trans. Appl. Supercond.*, **7**, 3147 (1997).
102. R.C. Black, F.C. Wellstood, E. Dantsker, A.H. Miklich, J.J. Kingston, D.T. Nemeth, and J. Clarke, *Appl. Phys. Lett.*, **64**, 1 (1994).
103. R.C. Black, F.C. Wellstood, E. Dantsker, A.H. Miklich, D. Koelle, F. Ludwig, and J. Clarke, *IEEE Trans. Appl. Supercond.*, **5**, 2137 (1995).
104. Y.R. Chemla, T.S. Lee, J.Clarke, M. Adamkiewicz, and B. Buchanan, in *Extended Abstracts of 6th International Superconductive Electronics Conference (ISEC'97)* Berlin, eds. H. Koch and S. Knappe, **1**, (1997) p. 140.
105. J. Clarke, *IEEE Trans. Magn.*, **MAG-19**, 288 (1983).
106. E. Dantsker, D. Koelle, A.H. Miklich, D.T. Nemeth, F. Ludwig, J. Clarke, J.T. Longo, and V. Vinetskiy, *Rev. Sci. Instrum.*, **65**, 3809 (1994).
107. U. Kalberkamp, U. Matzander, K.D. Husemann, G. Panaitov, E. Zimmermann, and Y. Zhang, *Appl. Supercond.*, **5**, 205 (1998).
108. M. Bick, G. Panaitov, Y. Zhang, H. Bousack, A.I. Braginski, U. Kalberkamp, H. Burkhardt, and U. Matzander, ''A HTS rf SQUID Vector Magnetometer for Geophysical Exploration Methods,'' Applied Superconductivity Conference (ASC'98), Palm Desert, CA; to be published in *IEEE Trans. Appl. Supercond.* **9**, (1999).